AGU PUBLICATIONS

Earth's Future

RESEARCH ARTICLE

10.1002/2014EF000270

Early signatures of ozone trend reversal over the Antarctic

Anita Várai[1], Viktória Homonnai[1], Imre M. Jánosi[1], and Rolf Müller[2]

[1]Department of Physics of Complex Systems, Eötvös Loránd University, Budapest, Hungary, [2]Forschungszentrum Jülich GmbH, Institute of Energy and Climate Research (IEK-7), Jülich, Germany

Key Points:
- There is a robust trend reversal observed for Antarctic total ozone
- The trend reversal is consistent with changing stratospheric halogen loading
- No close correspondence of ozone and halogen turn around

Corresponding author:
R. Müller, ro.mueller@fz-juelich.de

Citation:
Várai, A., V. Homonnai, I. M. Jánosi, and R. Müller (2015), Early signatures of ozone trend reversal over the Antarctic, *Earth's Future*, *3*, 95–109, doi:10.1002/2014EF000270.

Received 31 JUL 2014
Accepted 18 JAN 2015
Accepted article online 9 FEB 2015
Published online 4 MAR 2015

Abstract We report on a detailed time series analysis of long total column ozone (TO) records based on multi-satellite observations of daily resolution. We concentrate on three geographic latitudes over and around the Antarctic area, specifically on three circles at 58.5°S, 59.5°S, and 79.5°S. Almost continuous observations are available at the two former latitudes; however, data are lacking during the polar winter periods at 79.5°S, because the measurement technique requires sunlight. The methodology is motivated by level-crossing statistics, where subsets of the records above or below particular threshold levels are evaluated. Long-term trend reversal at around the turn of the century is already detectable for low TO levels in the raw time series in the "ozone-hole" region (79.5°S). In order to overcome the apparent non-stationarities of the time series, we determined daily TO differences (ΔTO) belonging to the same geographic longitudes between the different latitudinal circles. The result is a stable, stationary behavior for small (absolute) ΔTO values in the period January–February–March without any significant detectable trends. The high absolute value ΔTO subsets (September–October–November) indicate a robust trend reversal in the middle of the 1990s. The observed trend reversal in the total column ozone time series is consistent with the temporal development of the stratospheric halogen loading. However, a close correspondence of ozone and halogen turnaround years is not expected because of the statistical uncertainties in the determination of the ozone turnaround, and the many factors contributing to ozone depletion processes.

1. Introduction

Since the early 80s, extensive depletion of ozone has been observed over Antarctica each spring; this phenomenon is referred to as the "ozone hole" [*Farman et al*., 1985; *Stolarski et al*., 1986; *Solomon*, 1999]. It is well established that this depletion of ozone is ultimately caused by the increase of man-made chemicals in the atmosphere such as chlorofluorocarbons and halons that contain ozone-destroying chlorine and bromine [*Solomon*, 1999; *World Meteorological Organization (WMO)*, 2011, 2014]. As as consequence of the Montreal Protocol and its amendments and adjustments, the concentrations of most of the anthropogenic chlorine and bromine source gases are now declining in the troposphere [*WMO*, 2011, 2014]. Exceptions are shorter-lived halogen compounds (mostly introduced as replacement compounds for longer lived source gases), which do not substantially contribute to the stratospheric halogen loading.

A commonly employed measure of stratospheric halogen loading is the equivalent effective stratospheric chlorine (EESC), a quantity that allows the combined effect of halogen compounds (Cl and Br) on ozone to be estimated [*Daniel et al*., 1995; *Newman et al*., 2007; *WMO*, 2011]. This quantity is calculated by taking ground-based observations of halogen compounds (estimating the Cl and Br atoms in each compound), lagging the time with respect to transport into the stratosphere, estimating the conversion of these halogens to inorganic form, and then scaling the bromine because it is more efficient in destroying ozone [*Newman et al*., 2007].

The stratospheric halogen loading responds to tropospheric change with a delay of several years [*Hall et al*., 1999], with the delay being longer in the polar stratosphere than in the mid-latitude stratosphere. However, the stratospheric halogen loading is now decreasing throughout the stratosphere [*WMO*, 2011; *Montzka*, 2012; *Ko et al*., 2013]. Peak values of the stratospheric halogen loading were reached in the mid-latitude stratosphere in about 1997 and in the polar stratosphere in about 2002 [*WMO*, 2011].

As a consequence of the decline of the stratospheric halogen loading, first a leveling-off and later an increase of Antarctic spring ozone levels is expected. Model simulations project a return to 1980 total

ozone levels in Antarctic spring in about 2045–2060 and a peak in Antarctic ozone depletion around the year 2000 [*Eyring et al*., 2010; *WMO*, 2011, 2014].

However, substantial natural year-to-year variability in Antarctic column ozone caused by variability in Antarctic spring temperatures and dynamical conditions make it difficult to definitely detect a trend reversal in Antarctic spring ozone. Even more difficult is an unequivocal attribution of a change in Antarctic ozone to changes in EESC, because the effect of a reduction in EESC on Antarctic ozone columns is expected to be moderate during the first years after the EESC peak occurs in the stratosphere [*Newman et al*., 2006; *WMO*, 2011, 2014]. Furthermore, Antarctic ozone loss is not directly driven by EESC, but rather by inorganic chlorine. Of course, inorganic chlorine is related to EESC, but it also shows a substantial year-to-year variability, which translates into a variability of polar chemical ozone loss [*Strahan et al*., 2014].

The question of when Antarctic ozone recovery should be detectable is the subject of current scientific debate. *Yang et al*. [2008] reported a statistically significant leveling-off of total column ozone in Antarctica since 1997 and argue that this leveling-off coincides with the time when the chemical forcing of polar ozone loss stopped increasing. *Hassler et al*. [2011] analyzed October mean column ozone from ground-based measurements in Antarctica for the period 1966–2008 and did not find a trend reversal in Antarctic total column ozone. In contrast, *Salby et al*. [2011, 2012] reported a statistically significant increase in Antarctic spring ozone caused by the declining EESC, based on a removal of total ozone variations caused by dynamical processes from the observed time series. Furthermore, on the basis of multivariate regression analyzes based on several total ozone measurements for the period 1979–2010 and on different measures of Antarctic ozone loss, *Kuttippurath et al*. [2013] reported a statistically significant positive trend in Antarctic total ozone for the period 2000–2010. Recently, *de Laat et al*. [2015] revisited reports of observed increases in springtime Antarctic vortex mean total column ozone [*Salby et al*., 2011, 2012; *Kuttippurath et al*., 2013] and argued that, when considering uncertainties in the employed multivariant regressions, attributions of increases in Antarctic springtime ozone to decreasing stratospheric halogens are not warranted. Furthermore, *Kuttippurath et al*. [2015] argued that EESC-based regression is inappropriate for unambiguously detecting ozone recovery from the effects of stratospheric halogens, so that earlier EESC-based ozone trend results might need to be revised.

Here we follow a different approach to analyze Antarctic total ozone time series. Rather than using multivariate linear regression based on a number of proxies to describe processes known to affect Antarctic ozone (e.g., poleward heat flux or EESC), we conduct a time series analysis of the pure, unfiltered data set over the Antarctic. In particular, we do not prescribe a break year, either directly (as in a piecewise linear trend analysis), or indirectly by relating a trend in Antarctic ozone to EESC. Our methodology is based on level-crossing statistics, where subsets of the data record above and below particular threshold levels are evaluated [*Brainina*, 2013]. Using a variety of statistical trend analysis estimates, we find a robust trend reversal in Antarctic ozone with a turnaround in ozone in approximate agreement with the peak stratospheric halogen loading. The same statistical analysis was additionally performed on two difference time series, where daily mean total ozone (TO) differences were determined between a polar and two sub-Antarctic latitudes. In this way, we removed part of the seasonal cycle and many spatially extended effects (e.g., volcanic forcing) in the raw record of Antarctic total ozone. The difference time series mainly represent the rapid and widespread halogen-catalyzed ozone loss at polar latitudes, and they exhibit an earlier turning point than the raw record.

2. Data and Methods

Measured total column ozone (TO) data are obtained from a database (Version 3) compiled and maintained by Bodeker Scientific (http://www.bodekerscientific.com) from satellite and ground-based observations [*Bodeker et al*., 2005; *Müller et al*., 2008; *Struthers et al*., 2009]. Records span the time interval 1 November 1978 to 3 April 2011 over a global geographic grid of 1.0° × 1.25° (lat/lon). Missing satellite data are complemented by spatial linear interpolation [*Bodeker et al*., 2001a, 2001b]. Figure 1 illustrates our focus area along three entire latitudinal circles at 58.5°S, 59.5°S, and 79.5°S each formed by 288 longitudinal grid points.

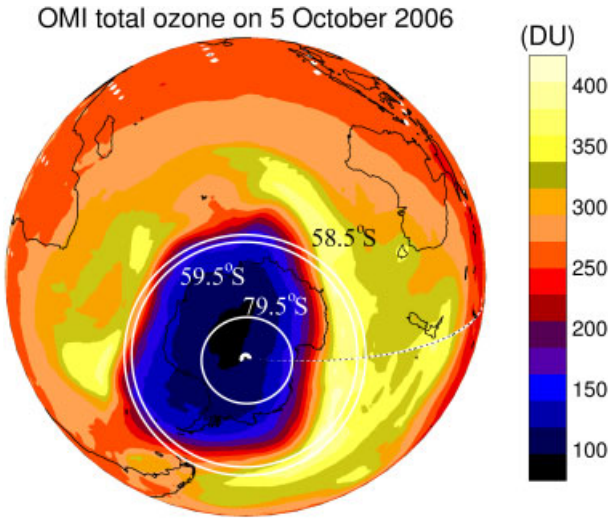

Figure 1. Latitudes where daily total column ozone values are analyzed over the Antarctic. (Underlying map shows OMI satellite total column ozone measurements [*Levelt et al.*, 2006] on 5 October 2006.)

The former two latitudes represent an almost continuous series of records: 11,656 days at 58.5°S and 11,648 days at 59.5°S for the whole period of 11,832 days (dates of less than 10 longitudinal observations are omitted from the statistics). Most satellite instruments monitoring total column ozone use backscattered solar radiation to estimate total ozone; therefore, data are available only for 6662 days at 79.5°S.

In order to decrease the effects of lacking or erroneous data points, a zonal average is calculated for each day together with the standard deviation, separately for the three latitudinal circles. The result is plotted in Figure 2 (note that the two upper curves are shifted upwards by 100 and 200 Dobson units (DU) for better visualization). The September–October low TO values at 79.5°S (red curve in Figure 2) clearly demonstrate the well-known "ozone-hole" phenomenon. The two other time series also exhibit a weaker but apparent non-stationary behavior; especially a slow overall decrease during the 1980s is obvious. This decrease is consistent with the observation that TO values at Southern Hemisphere mid-latitudes between 2004 and 2012 are about 6% lower than during 1964–1980 [*WMO*, 2014].

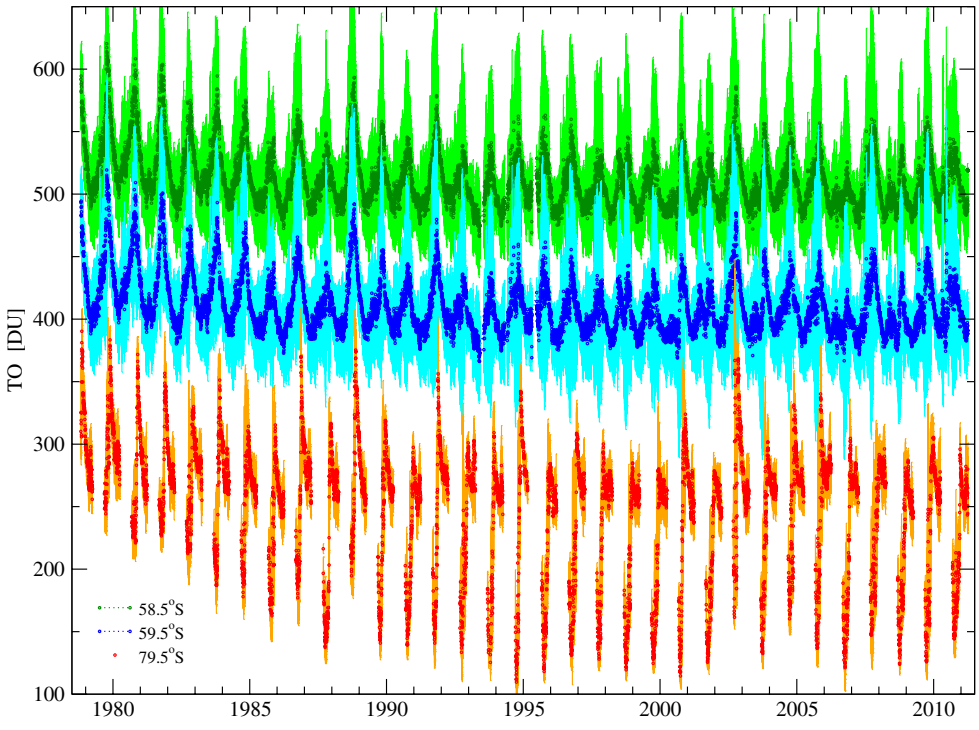

Figure 2. Zonal mean daily total column ozone ⟨TO⟩ averaged along the three latitudes 58.5°S (green), 59.5°S (blue), and 79.5°S (red). The former two series are shifted upward by 200 and 100 DU for better visualization. Colored bands represent standard deviations around the daily zonal mean values over 288 longitudes.

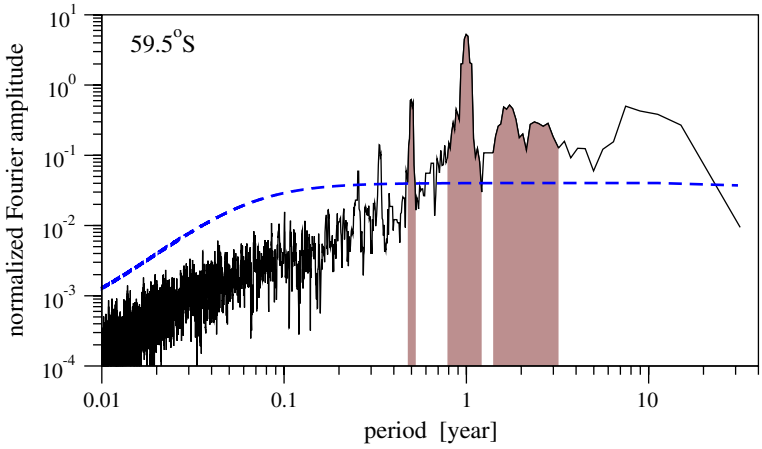

Figure 3. Normalized power spectrum of the mean TO time series recorded at 59.5°S on a double-logarithmic scale. Blue dashed line indicates the 95% confidence interval with respect to a red noise spectrum. Shaded areas represent the spectral weights of semiannual (6.05%), annual (56.89%), and quasi-biennial oscillations (11.51% of the total variance).

The strong similarities between the two sub-Antarctic time series might suggest that their joint analysis provides redundant information. However, a closer look reveals that daily mean TO values at 59.5°S are systematically lower by 10–15 DU than at 58.5°S during the autumn periods, indicating a visible influence of the polar ozone loss. Indeed, the results of trend reversal tests are slightly different for these two close latitudes, as we will demonstrate later.

Spectral analysis can provide detailed information on the temporal behavior of the TO signals, besides the deterministic annual oscillations. We determined the power spectra of the time series at 58.5°S and 59.5°S by the multitaper method [*Mann and Lees*, 1996], which is largely unbiased by the presence of signals immersed in a "red" noise background arising from temporal persistence. As the two spectra are practically identical, we show data only for 59.5°S (Figure 3). It is well known that the dominant annual cycle is accompanied by semiannual and quasi-biennial oscillations (QBOs) together explaining about 75% of the whole variability (note that spectral weight estimation and normalization are performed in the frequency scale, while the result is shown on a reciprocal scale in units of period of years). No conclusions can be derived for oscillations for large periods of many years (in particular not for an 11 year periodicity) due to the length of the record and the inherent non-stationarity of the background. The usual procedure is to filter out these spectral bands and decompose effects of assumed explanatory variables such as solar cycle, volcanic activity, and stratospheric temperature [e.g., *Salby et al*., 2012]. However, we do not follow this practice in this study for two reasons. First, we would like to avoid any unintended distortion of the signals; therefore, we restrict our pretreatment to the minimal level described below. Second, the ozone hole is a phenomenon of unusually low TO levels, and any trend reversal must be manifested in a change of this quantity, whatever its physical mechanism.

A useful way of characterizing strongly fluctuating signals is based on level-crossing statistics [*Brainina*, 2013]. Here we adopt one particular aspect of the statistical toolbox by dividing the signals into subsets where the values ascend above or drop below a given threshold level. Usual quantities of interest are the distribution functions and correlation properties of level-crossing and level-exceedance events; however, the restricted length of ozone records prevents such information being extracted with acceptable confidence. (Many practical questions can be answered by level-crossing statistics, such as those related to the probability of crossing a given water level in rivers, crossing concentration levels of dangerous pollutants, or critical wind speeds for turbine construction). In our analysis, we begin with the following main assumption: when a robust trend reversal can be detected in a given subset of an ozone record, this behavior must not be sensitive to the particular choice of the threshold level determining the subset. We implement three different methods in order to detect a possible trend reversal in the time series.

First, quadratic fitting is performed by the chi-square method [*Press et al*., 1992] by minimizing the quantity:

$$\chi^2 = \sum_{i=1}^{N} \left[\frac{\langle \mathrm{TO} \rangle_{l,i} - \left(a + bt_i + ct_i^2 \right)}{\sigma_{l,i}} \right]^2, \quad (1)$$

where $\langle \mathrm{TO} \rangle_{l,i}$ is the zonal mean of total column ozone (TO) over 288 longitudes at a given latitude on day i. The standard deviation is denoted by $\sigma_{l,i}$, and the normal form of a quadratic polynomial

$$x(t) = a + bt + ct^2. \tag{2}$$

is used with coefficients a, b, and c. For easier evaluation of fitted parabolas, we evaluate the vertex form of Equation (2):

$$x(t) = c\left(t - t_0\right)^2 + h, \tag{3}$$

where t_0 is the location of the vertex (representing a minimum when the quadratic coefficient c is positive), and h is the shift parameter along the axis x. The cross relations between the coefficients of Equations (2) and (3) are

$$t_0 = -\frac{b}{2c}, \quad h = a - \frac{b^2}{4c}. \tag{4}$$

One drawback of detecting a trend reversal by quadratic fitting is related to the symmetry of a parabola. In order to overcome this limitation and permit different slopes of decreasing and increasing trends, we implement two further methods to perform broken-stick fits for the ozone record [*Toms and Lesperance*, 2003]

The simplest piecewise linear regression model joins two straight line segments exactly at a given breakpoint α_{bs} as follows:

$$x\left(t_i\right) = \begin{cases} \beta_0 + \beta_1 t_i & \text{for} \quad t_i < \alpha_{bs} \\ \beta_0 + \beta_1 t_i + \beta_2\left(t_i - \alpha_{bs}\right) & \text{for} \quad t_i \geq \alpha_{bs}. \end{cases} \tag{5}$$

The slopes of the line segments are β_1 and $\beta_1 + \beta_2$. It is clear that such a piecewise linear fit can be performed only by some nonlinear algorithm; here we use the well-known Nelder–Mead simplex method developed for nonlinear optimization [*Mathews and Fink*, 2004].

The target to be minimized is again a χ^2 value defined in analogy with Equation (1), that is, the sum of the squared error between the fitted and recorded data weighted by the zonal standard deviation for a given day. Note that the number of fitted coefficients is increased by 1 compared with the simple parabolic fit of three free parameters.

The third method further increases the number of free parameters, but it provides a continuous joining of two linear segments by incorporating a hyperbolic tangent function:

$$x\left(t_i\right) = \gamma_0 + \gamma_1\left(t_i - \alpha_c\right) + \gamma_2\left(t_i - \alpha_c\right)\tanh\left(\frac{t_i - \alpha_c}{\delta}\right), \tag{6}$$

where α_c denotes the smooth-transition breakpoint, and the new parameter δ controls the sharpness of the transition. Since our goal is simply to detect trend reversal and check its robustness, we fix the value $\delta = 0.001$ resulting in a similarly sharp joining of two linear segments as in the previous model Equation (5). In this case, we exploit the Levenberg–Marquardt algorithm [*Press et al*., 1992], as the closed form of Equation (6) is continuous everywhere.

The main assumption of a single turning point at each method might seem to be rather restrictive and too simplistic to describe such complex TO signals as plotted in Figure 2. However, we do not know all the chemical and physical processes explaining variability and small fluctuations, thus there is no additional information gained when the signal is fitted by, for example, a 10th order polynomial.

3. Results

As a first step, we concentrate on the time series shown in Figure 2 by red symbols, that is, the zonal daily mean TO levels along 79.5°S. Figure 4 illustrates the results of quadratic chi-square fitting for four subsets of the signal representing the ozone-hole phenomenon. The lower the threshold value $\mathrm{TO}_{\mathrm{th}}$, the earlier the timing of the vertex. Values range between 2000.6 and 1999.1, which is in rough agreement with the timing found by *Salby et al*. [2012]. Note that the quadratic parameter c seems to depend strongly on the threshold value; therefore, we extend the analysis by fitting each individual subset separated by 1 DU

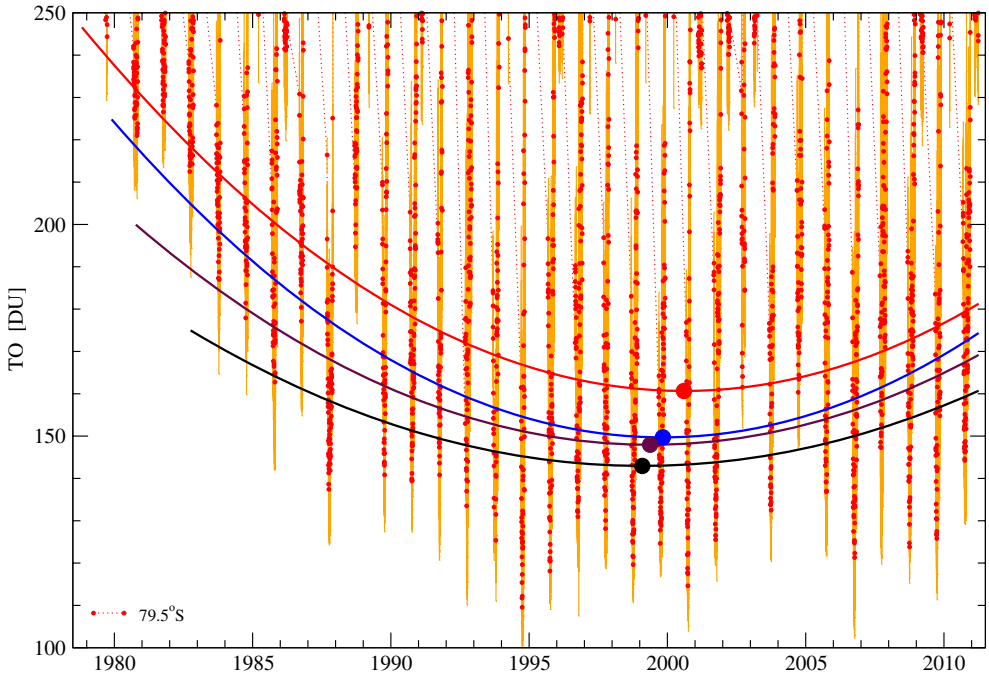

Figure 4. Quadratic fits for four different subsets of the zonal mean daily time series at 79.5°S ($N = 6662$ data points): TO < 250 DU ($N_{250} = 2312$), red line; TO < 225 DU ($N_{225} = 1831$), blue line. TO < 200 DU ($N_{200} = 1454$), maroon line; TO < 175 DU ($N_{175} = 961$), black line. Solid circles indicate the minimum values at 2000.6, 1999.8, 1999.4, and 1999.1.

below and above 250 DU where at least 400 data points are recorded. The choice of 250 DU for cutting the time series into a lower and an upper section is somewhat arbitrary; however, we will return to this point below.

Summary statistics are shown in Figure 5, where the dependencies of the temporal location of the vertex t_0, the number of data points N_{th}, and the fitted value of the quadratic coefficient c on the threshold value TO_{th} are shown. Notable features are the following. The location of the vertex remains in a narrow range around $\bar{t}_0 = 1999.6 \pm 0.5$ in the lower section (250 DU > TO_{th} > 160 DU); however, a small systematic shift as a function of the threshold value TO_{th} is apparent for t_0 (see Figure 5a, red curve). A similar, but more pronounced systematic shift is found for the quadratic coefficient c (Figure 5c, red curve). Furthermore, as expected, the higher the threshold, the larger the number of data points N_{th} in a given subset (Figure 5b). In the upper section (250 DU < TO_{th} < 320 DU), the stability of the vertex location breaks down

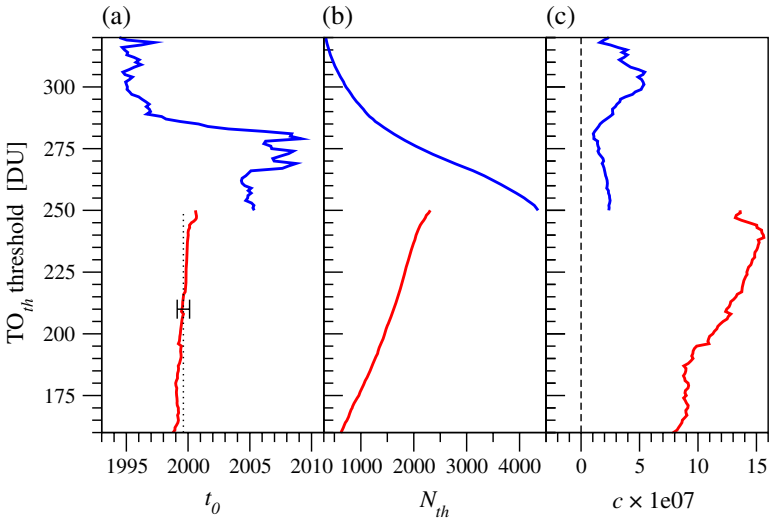

Figure 5. Statistics of χ^2 quadratic fitting for the upper subsets obeying TO > TO_{th} in the range 250 DU < TO_{th} < 320 DU (blue curves), and lower subsets of TO < TO_{th} in the range 250 DU > TO_{th} > 160 DU (red curves). (a) Location parameter t_0 [see Equation (3)], dotted line denotes the mean value for the lower subsets $\bar{t}_0 = 1999.6 \pm 0.5$. (b) Number of data points N_{th} in the subsets as a function of TO_{th} threshold levels for both subsets. (c) The quadratic coefficient c multiplied by 10^7 [see Equation (3)].

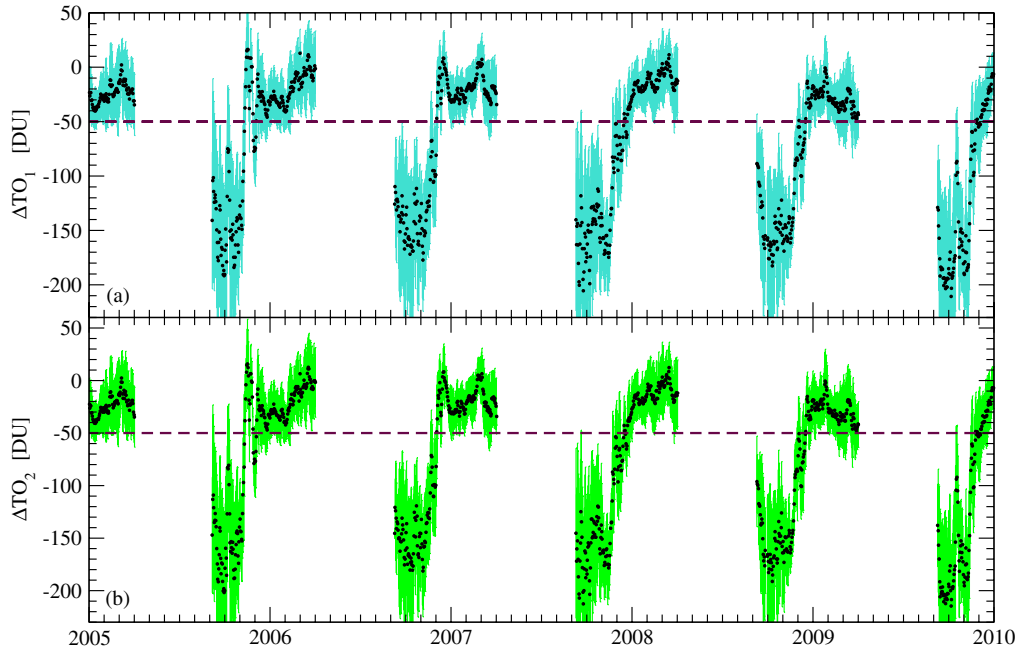

Figure 6. Five years of the difference times series for (a) $\Delta TO_1 = TO(79.5°S) - TO(59.5°S)$ and (b) $\Delta TO_2 = TO(79.5°S) - TO(58.5°S)$. Colored bands denote the standard deviation around the daily zonal mean value.

(Figure 5a, blue curve), but the sign of the quadratic parameter *c* remains positive (see Figure 5c, blue curve). These features suggest that the strong non-stationarity of the record clearly seen in Figure 2 gives a systematic bias of the results in the subsets of different threshold values.

Stationarity of a time series means that all statistical properties of a finite piece of the signal are independent of the starting time of the sample. Obviously, this is not true for the records in Figure 2, annual minima and maxima, the mean value, even the local variance on different days are fluctuate strongly, not to mention the apparent long-range trends. In order to reduce the effects of non-stationarities, we determine the difference of daily TO values between the polar latitude 79.5°S and the two near-continuous records at 59.5°S (ΔTO_1) and 58.5°S (ΔTO_2). This is based on the main assumption that at least two families of processes determine the absolute value of TO: one of which is responsible for the decline in sub-Antarctic and mid-latitude ozone, and the other causes the ozone hole itself over the Antarctic. The differences are computed for each longitude separately, and the zonal mean and the standard deviation are stored for each day where at least 10 longitudes contribute to the mean value. The result (see Figure 6) is two time series where a simple visual check permits an almost stationary upper section of $\Delta TO > -50$ DU and a lower section of $\Delta TO < -50$ DU to be separated. The two sections almost perfectly coincide with a high Antarctic-TO period of January–March and a low Antarctic-TO period of September–November with a transient (quick TO increase) during December. The low Antarctic-TO period in September–November coincides with the time when the Antarctic polar vortex prevails, whereas the high Antarctic-TO period in January–March coincides with the period when no vortex is present. In the following, we will concentrate on the trend analysis of these difference time series.

3.1. Chi-Square Quadratic Fits for ΔTO Time Series

As an example, we show the whole difference time series ΔTO_1 and five quadratic fits in Figure 7. The upper section $\Delta TO > -50$ DU seems to be nearly stationary supported by the brown fitted line, which has a vanishingly small quadratic coefficient *c*. This suggests that the general (weaker) background decline of the raw TO time series is not strongly dependent on latitude. The temporal locations of the vertex points are shifted to earlier times (compared to the raw time series, Figure 4) in the lower section $\Delta TO < -50$ DU. However, this behavior is expected, as the upper envelope of all three curves of the raw records in Figure 2 has a declining tendency, which is removed by forming the ΔTO series. The results for ΔTO_2 are very similar; therefore, they are represented in the summary statistics below.

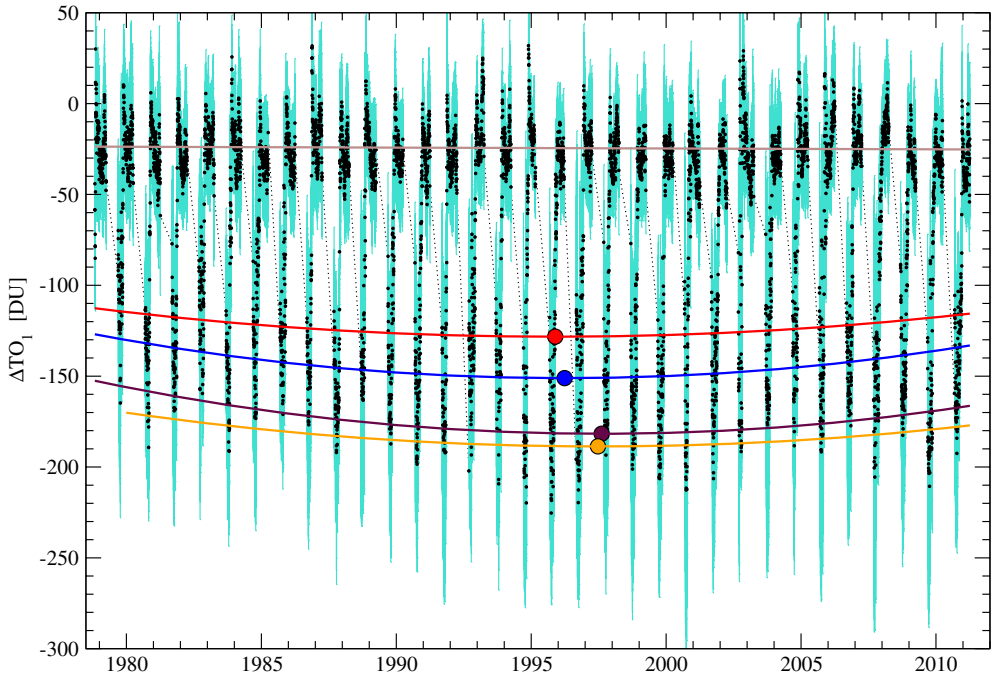

Figure 7. Quadratic fits for five subsets of the daily mean difference $\Delta TO_1 = TO(79.5°S) - TO(59.5°S)$. The topmost (brown) fit represents the subset of $\Delta TO_{th} > -50$ DU and it is practically trendless. The red, blue, maroon, and orange curves are quadratic fits for the subsets $\Delta TO_{th} < -50$ DU, $\Delta TO_{th} < -100$ DU, $\Delta TO_{th} < -140$ DU, and $\Delta TO_{th} < -170$ DU. The number of fitted points from the total of 6661 are 2536, 2022, 1248, and 472. The trend reversal points are 1995.9, 1996.2, 1997.6, and 1997.5 years (solid circles).

We repeated the same systematic procedure of fitting for both sections as shown in Figure 5. A few essential differences can be identified by comparing the results for the raw data and the difference time series. The ensemble mean value of the location parameter t_0 (vertex) appears two and a half years earlier, at around the beginning of 1997, if the daily ozone difference values are considered (Figure 8a). The quadratic coefficient c in the upper section is negligibly small, indicating an almost linear (actually almost horizontal) fit for both ΔTO_1 and ΔTO_2; it even has a small negative value for the highest subsets $\Delta TO_{th} > -20$ DU (Figure 8c). In the lower section, the coefficient c is remarkably stable for a wide range of threshold values compared with a fit for the raw data record (Figure 5c). Such enhanced stability is expected for both the upper and lower sections of the difference signals as a consequence of removing the background ozone decline.

With respect to the goodness of quadratic fits, it is illuminating to compare the values of reduced chi-square $\chi_r^2 = \chi^2 / (N_{th} - 4)$ (here N_{th} is the number of observations in a subset of a given threshold value TO_{th} or ΔTO_{th}, and the constant 4 belongs to a three-parameter fit) for the raw and the two difference time series (Figure 9). Values $\chi_r^2 \lesssim 1 - 1.5$ indicate acceptable quality; this condition is fulfilled only for a restricted threshold value range for the original measured signal at 79.5°S (see Figure 9c). Strongly decreasing values for χ_r^2 are expected for very low or very high thresholds, as the available range of data becomes narrower and narrower, and fits are increasingly restricted to the upper and lower envelopes of the records.

3.2. Broken-Stick Fits by Nelder–Mead Method

Trend reversals are often detected by various broken-stick fits such as those given in Equation (5). The Nelder–Mead simplex method is used to perform fits in both the upper and lower sections of the TO difference time series; examples are shown in Figure 10. The algorithm is an unconstrained nonlinear optimization method; that is, we cannot give upper or lower bounds for parameters. It is known that fitted parameter values can converge to non-stationary points [*Lagarias et al*., 1998; *McKinnon*, 1998]; therefore, iterations are performed from 50 initial guess values of the breakpoint parameter α_{bs} [see Equation (5)] distributed evenly in the temporal range 1979–2011 for each individual threshold value $\Delta TO_{th,1}$ and $\Delta TO_{th,2}$. Summary statistics are presented in Figures 11 and 12.

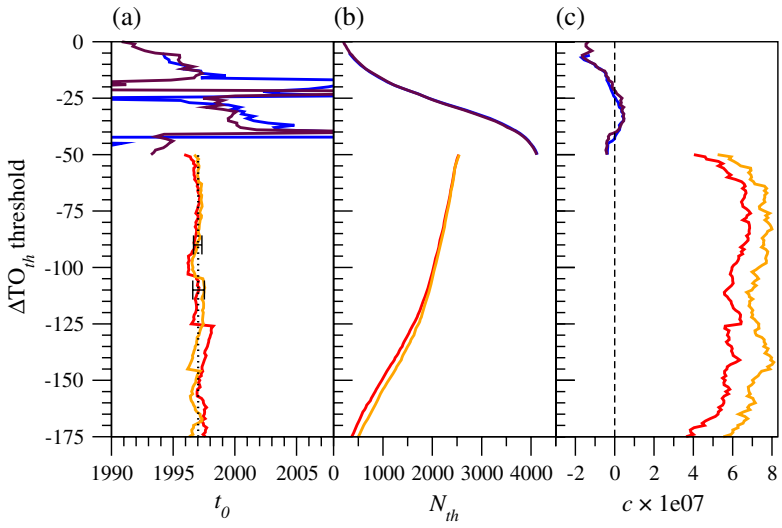

Figure 8. Statistics of χ^2 quadratic fitting for the upper subsets obeying $\Delta TO > \Delta TO_{th}$ in the range -50 DU $< \Delta TO_{th} < 0$ DU (blue ΔTO_1, maroon ΔTO_2), and lower subsets of $\Delta TO < \Delta TO_{th}$ in the range -175 DU $< TO_{th} < -50$ DU (red ΔTO_1, orange ΔTO_2). (a) Location parameter t_0 [see Equation (3)], dotted lines denote the mean value for the lower subsets $\overline{t}_0 = 1997.1 \pm 0.5$ year (ΔTO_1) and $\overline{t}_0 = 1997.0 \pm 0.3$ year (ΔTO_2). (b) Number of data points N_{th} in the subsets as a function of ΔTO_{th} threshold levels for both subsets. (c) The quadratic coefficient c multiplied by 10^7 [see Equation (3)].

The general behavior is very similar to the chi-square quadratic fits. The lower sections ($\Delta TO_{th} < -50$ DU) exhibit stronger stability than the upper sections ($\Delta TO_{th} > -50$ DU) considering the location of the breakpoint (Figures 11a and 12a). The ensemble mean value of trend reversal is around 1995 for both TO difference time series in the lower sections (precisely $\overline{\alpha}_{bs,1} = 1994.6 \pm 1.7$ and $\overline{\alpha}_{bs,2} = 1995.5 \pm 1.4$), which is some 2 years earlier than that observed for the quadratic fits (see Figure 8). Consistency is also observed in the slopes of line segments (Figures 11b and 12b). However, an enhanced instability is found for subsets -91 DU $< \Delta TO_{th,1} < -73$ DU illustrating the sensitivity of the convergence in noisy time series. Interestingly, this unstable threshold range is not present in the second difference subsets of ΔTO_2 (see Figure 12b).

3.3. Continuous Broken-Stick Fits by Levenberg–Marquardt Algorithm

The smoothly joined line segments in a closed form given in Equation (6) consist of five parameters. As our main goal is to find a consistent trend reversal point instead of the best operational fitting function, we fixed the sharpness parameter $\delta = 0.001$ in order to shrink the parameter space. The

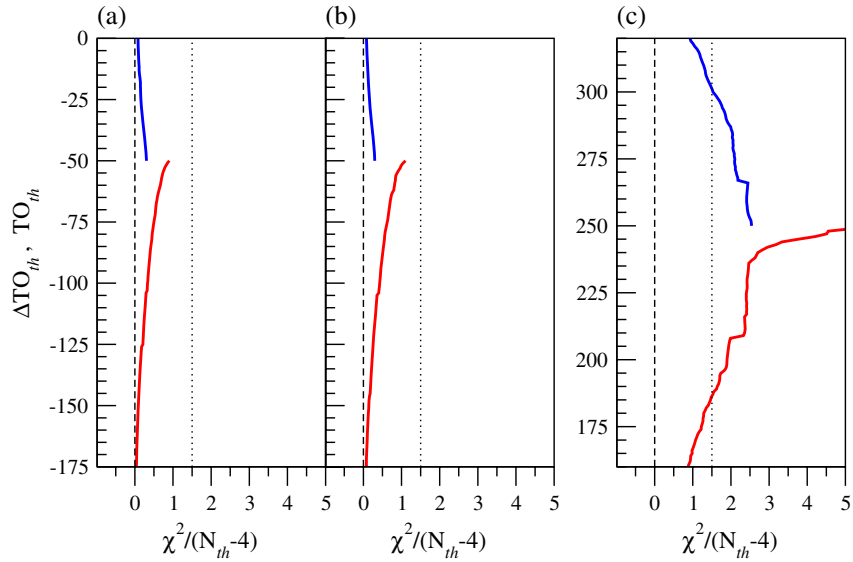

Figure 9. Goodness of fit characterized by the reduced chi-square parameter $\chi^2/(N_{th} - 4)$, where the denominator is the degrees of freedom for a three-parameter fit. (a) $\Delta TO_{th,1}$, (b) $\Delta TO_{th,2}$, (c) TO_{th} for the raw time series at 79.5°S.

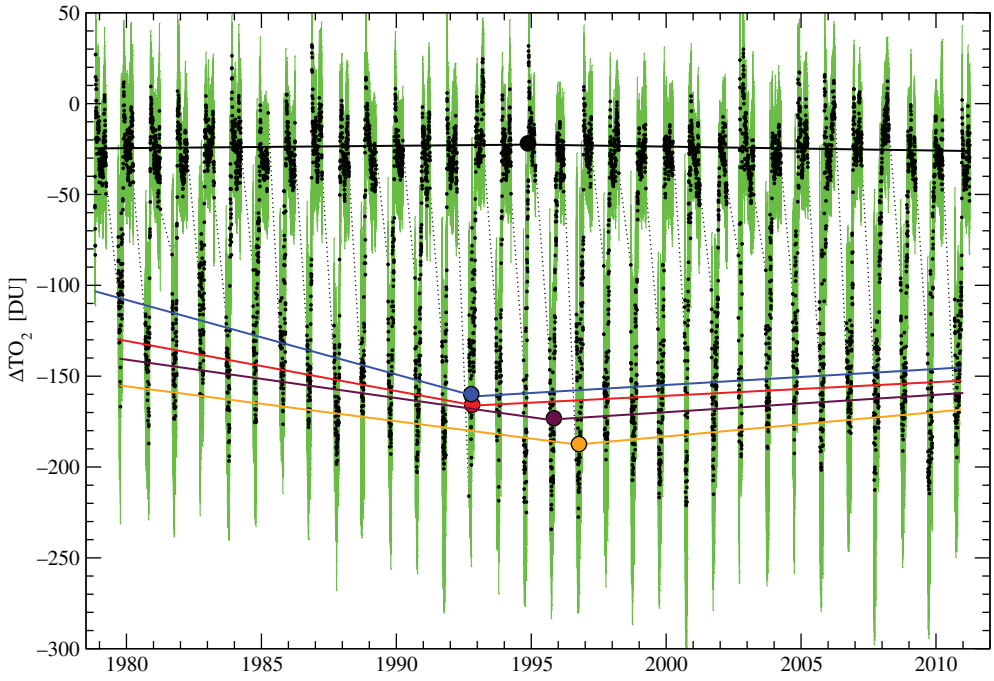

Figure 10. Nelder–Mead broken-stick fits [see Equation (5)] for five subsets of the daily mean difference $\Delta TO_2 = TO(79.5°S) - TO(58.5°S)$. The topmost (black) fit represents the subset of $\Delta TO_{th} > -50$ DU and is almost trendless with a detected breakpoint at $\alpha_{bs} \approx 1994.9$. The blue, red, maroon, and orange curves are fits for the subsets $\Delta TO_{th} < -75$ DU, $\Delta TO_{th} < -100$ DU, $\Delta TO_{th} < -125$ DU, and $\Delta TO_{th} < -150$ DU. The number of fitted points from the total of 6661 are 2288, 2022, 1617, and 973. The trend reversal points are 1992.9, 1992.9, 1995.6, and 1996.7 years (solid circles).

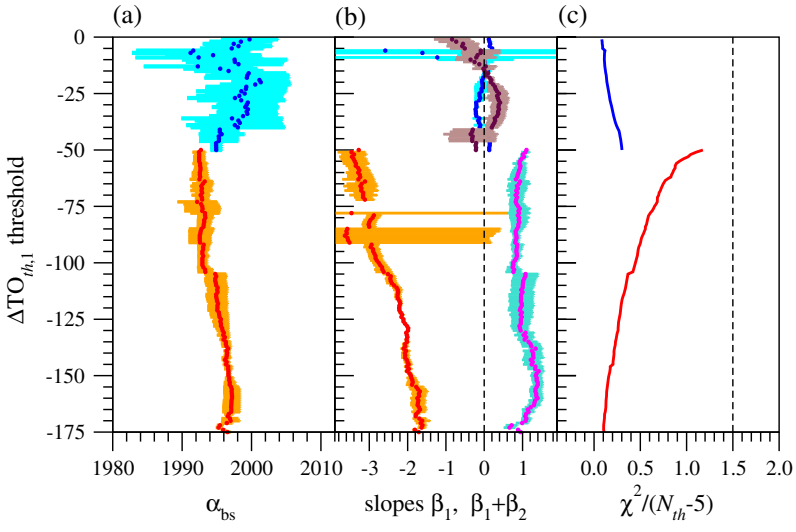

Figure 11. Statistics of Nelder–Mead broken-stick fits for the upper subsets obeying $\Delta TO_1 > \Delta TO_{th,1}$ in the range -50 DU $< \Delta TO_{th,1} < 0$ DU (blue), and lower subsets of $\Delta TO_1 < \Delta TO_{th,1}$ in the range -175 DU $< TO_{th,1} < -50$ DU (red). (a) Breakpoint parameter α_{bs} [see Equation (5)]. (b) Slopes β_1 (red, blue) and $\beta_1 + \beta_2$ (magenta, maroon) in the subsets as a function of threshold levels $\Delta TO_{th,1}$ for both sections. (c) Reduced chi-square $\chi_r^2 = \chi^2/(N_{th} - 5)$. Horizontal error bars in (a) and (b) are obtained from 50 initial guess values for the breakpoint parameter α_{bs}.

Levenberg–Marquardt algorithm is a standard of nonlinear optimization, and it is a constrained method (parameter values can be limited by defining boundary values). Example fits of Equation (6) are plotted in Figure 13.

With respect to an ensemble analysis, the same procedure is repeated as in the previous case for Nelder–Mead broken-stick fits. Although the convergence properties of the Levenberg–Marquardt method are considered to be superior to other algorithms, we tested its performance again from 50 initial guess values of the breakpoint α_c in the interval of 1979–2011. The summary statistics for the two TO difference series are presented in Figures 14 and 15. The breakpoint parameters α_c are shifted to an even earlier interval ($\overline{\alpha}_{c,1} = 1994.2 \pm 1.9$ and $\overline{\alpha}_{c,2} = 1992.7 \pm 1.4$). It is interesting to note that when we do not fix the sharpness

parameter $\delta = 0.001$ in Equation (6), the five-parameter fits hardly change. Even at values $\delta \approx 1$, the fitted curves are broken sticks with practically the same slopes and breakpoints.

4. Discussion

In the previous sections, we demonstrated the following properties of daily total ozone time series averaged along three geographic latitudes in the period 1 November 1978 to 3 April 2011.

1. The record at the polar latitude 79.5°S exhibits a marked turning point for low ozone levels in each subset obeying $TO < TO_{th} \leq 250$ DU at around the end of the last century (Figure 4). The turning points are detected by simple chi-square quadratic fits, where the weights $1/\sigma_i$ for a given day i are obtained from the standard deviation around the mean of 288 longitudinal data points [Equation (1)].
2. In order to overcome the apparent non-stationarities of the records at the three latitudes incorporated in the analysis, two difference time series are determined between the polar circle 79.5°S and two lower latitudes 59.5°S and 58.5°S of almost continuous total ozone data. The difference time series have an almost stationary upper section $\Delta TO > -50$ DU (Figures 6 and 7). The quadratic fits for each threshold value in the lower sections exhibit an enhanced stability (Figures 6 and 7), and the turning point range is shifted to the middle of the last decade of the twentieth century (more precisely, to around 1997).
3. In order to permit different slopes for the ozone-hole formation and possible recovery periods, we implemented two different broken-stick fitting procedures, both of which are standard iterative, nonlinear optimization algorithms (Nelder–Mead, and Levenberg–Marquardt).
4. Iterative optimizations for noisy time series often determine a locally stable point instead of the actual turning point. Thus, we found that the most sensitive initial guess value is the breakpoint itself. For this reason, we determined mean parameter values and their standard errors from 50 initial breakpoint locations evenly distributed over the whole time period.
5. Both methods detect stable trend reversal in the lower subsets of both difference time series with consistent slopes (Figures 11, 12, 14, and 15). Mean trend reversal points are located in a slightly earlier period than identified by the symmetric parabolic fits, already in the first part of the 1990s.

With respect to the robustness of our results, we have performed the following test. There are a few years where geophysical events affected ozone levels, such as the eruption of Mt. Pinatubo in 1991 [*Rodriguez et al*., 1994; *Tie and Brasseur*, 1995; *Tilmes et al*., 2008] or the sudden stratospheric warming and ozone-hole split in 2002 [*Allen et al*., 2003; *Grooß et al*., 2005].

To demonstrate that these events do not substantially influence the result for the turnaround year $\bar{t}_0$, we determined the mean local minima by chi-square quadratic fits for the lower section

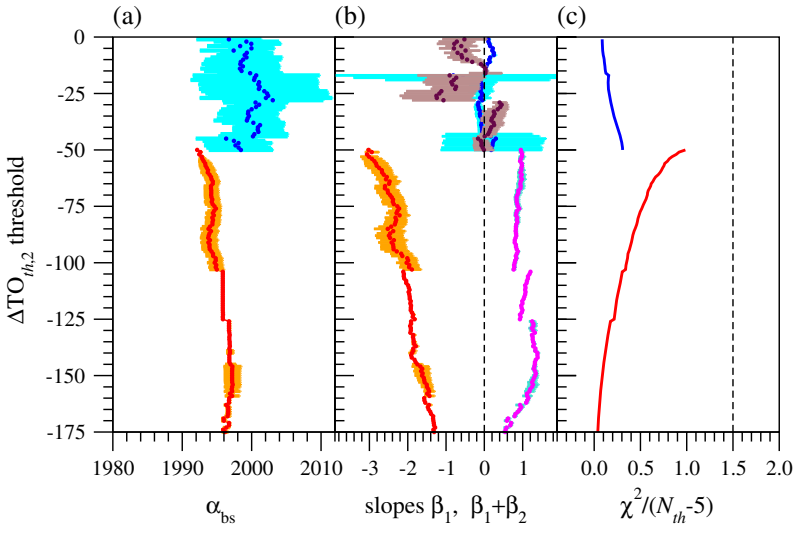

Figure 12. As Figure 11, but for the second difference time series ΔTO_2.

($-175 \leq \Delta TO_{th} \leq -50$ DU) of two truncated time series: one where the whole year of 2002, and another where years 1992–1994 and 2002 were removed. The results are negligibly changed, the numerical values are $\bar{t}_0 = 1997.1 \pm 0.5$ (full record) 1996.9 ± 0.6 (year 2002 is excluded), and 1997.0 ± 0.9 (4 years are excluded) for ΔTO_1, furthermore $\bar{t}_0 = 1997.9 \pm 0.3$ (full

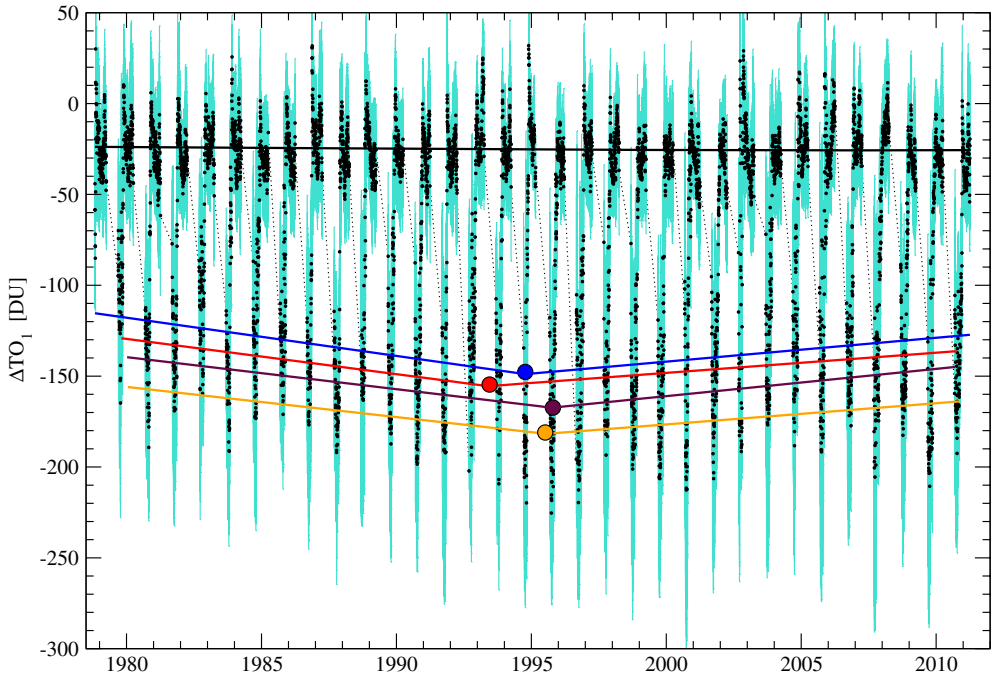

Figure 13. Levenberg–Marquardt fits [see Equation (6)] for five subsets of the daily mean difference $\Delta TO_1 = TO(79.5°S) - TO(59.5°S)$. The topmost (black) fit represents the subset of $\Delta TO_{th} > -50$ DU and is practically trendless (breakpoint is far outside the plotted time interval). The blue, red, maroon, and orange curves are fits for the subsets $\Delta TO_{th} < -75$ DU, $\Delta TO_{th} < -100$ DU, $\Delta TO_{th} < -125$ DU, and $\Delta TO_{th} < -150$ DU. The number of fitted points from the total of 6661 are 2288, 2022, 1617, and 973. The trend reversal points are 1994.8, 1993.4, 1995.8, and 1995.6 years (solid circles).

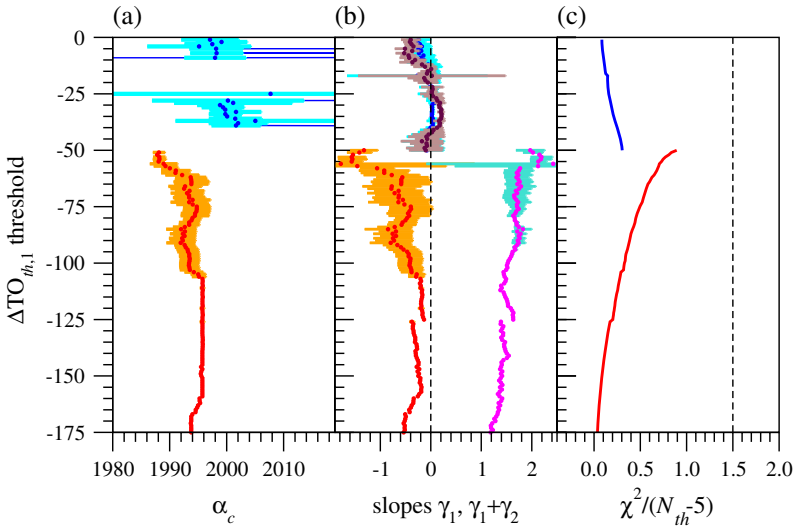

Figure 14. Statistics of Levenberg–Marquardt continuous broken-stick fits for the upper subsets obeying $\Delta TO_1 > \Delta TO_{th,1}$ in the range -50 DU $< \Delta TO_{th,1} < 0$ DU (blue), and lower subsets of $\Delta TO_1 < \Delta TO_{th,1}$ in the range -175 DU $< TO_{th,1} < -50$ DU (red). (a) Breakpoint parameter α_c [see Equation (6)]. (b) Slopes γ_1 (red, blue) and $\gamma_1 + \gamma_2$ (magenta, maroon) in the subsets as a function of threshold levels $\Delta TO_{th,1}$ for both sections. (c) Reduced chi-square $\chi_r^2 = \chi^2 / (N_{th} - 5)$. Horizontal error bars in (a) and (b) are obtained from 50 initial guess values for the breakpoint parameter α_{bs}.

record), 1996.9 ± 0.3 (year 2002 is excluded), and 1997.4 ± 0.6 (4 years are excluded) for ΔTO_2.

As a second stability test, we implemented data shuffling for the difference time series in the following way. Figures 6 and 7 illustrate strong seasonality and long periods of missing data (as a consequence of the polar winter in the Antarctic). Thus we cut whole years at 31 December (the first and last partial years are omitted), and randomly shuffled them to form an artificial time series. We repeated the same trend reversal location tests as before, the results for chi-square quadratic fits are illustrated in Figure 16.

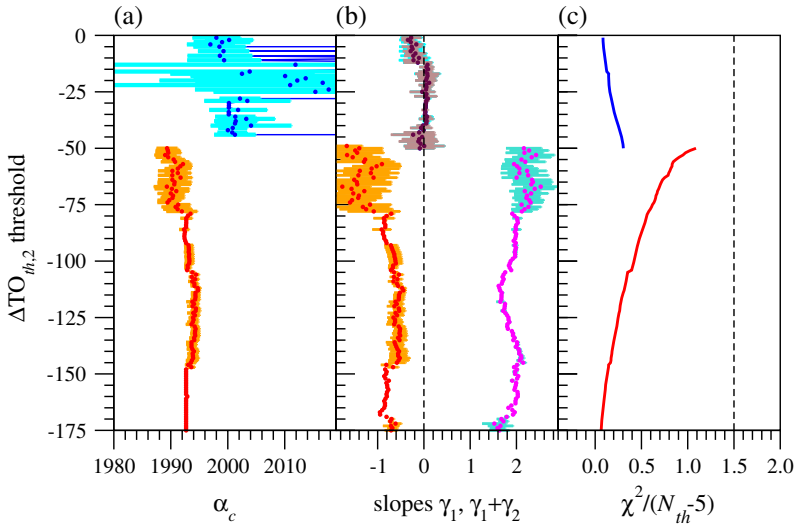

Figure 15. Same as Figure 14, but for the second difference time series ΔTO_2.

Figure 16a is a scatter plot for the mean turning point (vertex) and its standard deviation over 125 different subsets of different threshold values. While many of the randomly shuffled records have a vertex located around the beginning of the 21st century, their mean error is significantly larger than for the measured data (crosses in Figure 16a). The logarithmic vertical scale should be noted. It is even more informative that a large fraction of shuffled records have a near zero or even negative quadratic coefficient *c* (Figure 16b), here the measured record (crosses) likewise represent outliers. Finally, Figure 16c illustrates that although shuffled records cannot be easily recognized as artificial products, fits to level-crossing subsets still exhibit an inconsistent picture: the mean turning point is fully outside the measured interval with an enormous standard error (orange square in Figure 16a).

Finally, we return to the point of minimizing any prefiltering, and decomposing the measured data by proxies describing processes known to affect Antarctic ozone, e.g., QBO or volcanic activity. Especially the QBO contribution for the total ozone levels is routinely removed [e.g., *WMO*, 2011; *Salby et al*., 2011, 2012], although a recent study indicates that removing, for example, the QBO signal tends to increase rather than decrease the overall uncertainty in trend analysis for Antarctic ozone [*de Laat et al.*, 2015].

Here we did not follow the practice of removing a QBO component (or any other components) from the ozone record. Note that the QBO component is almost periodic with an almost constant amplitude, and the removal of such a signal from our time series where practically half-year cuts (polar night periods) are present cannot considerably affect the final results. The noise level and sensitivity of the iterative breakpoint search contribute much more strongly to the statistical uncertainties.

5. Conclusions

We analyzed time series of Antarctic total ozone for signatures of trend reversal based on level-crossing statistical techniques. In contrast to earlier studies, we do not remove components of total ozone variability (e.g., QBO or volcanic activity) from the ozone time series, and we do not prescribe a turning point for Antarctic total ozone in the analysis.

For total ozone at 79.5°S, we find a clear trend reversal with a turning point around the year 2000. For the lower section of the difference time series (difference between 79.5°S and two lower latitudes 59.5°S and 58.5°S), which coincides with data from the September–November period, we likewise find clear turning points. These turning points are more stable than those derived from the raw record of polar TO (i.e., less dependent on the required initial guess values) and lie in the early and mid-1990s, depending on the statistical technique employed. Thus, we conclude that a robust statistical signal of a trend reversal is present in the Antarctic total ozone record (1978–2011) analyzed here. However, an accurate determination of the year of the turning point is not possible because of the statistical uncertainties of the record.

Our closing remark is related to EESC, a measure of the stratospheric halogen loading, as already mentioned in Section 1. In Figure 17 we plotted two characteristic EESC curves available at the Goddard Space Flight Center data bank (http://acd-ext.gsfc.nasa.gov/). It is important to avoid any overinterpretation,

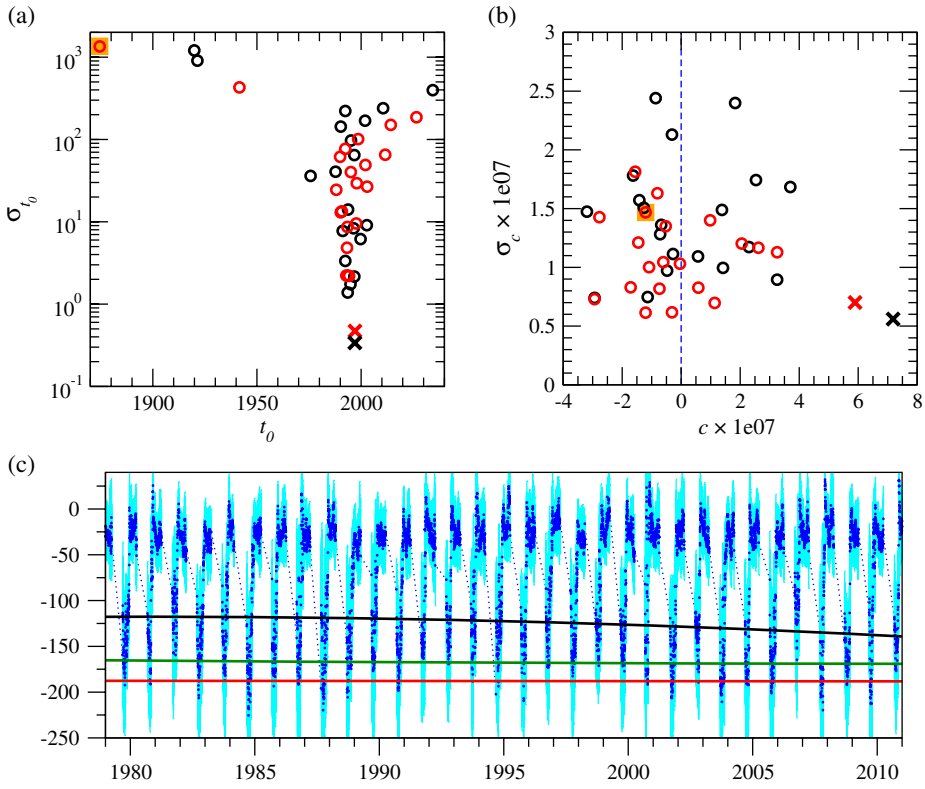

Figure 16. Statistics for 20 realizations of randomly shuffled years of both ΔTO records, the lower subsets in the range −175 DU > TO_{th} > −50 DU are evaluated by χ^2 quadratic fitting. (a) Scatter plot of the mean vertex point $\bar{t}_0$ and its standard deviation (red circles for ΔTO_1, and black circles for ΔTO_2). Crosses denote the results obtained from the original time series. (b) Mean quadratic coefficient c multiplied by 10^7 [see Equation (3)] versus its standard deviation (same notation). (c) One example of randomly shuffled years (ΔTO_1) representing extremely unstable quadratic fits for the lower subset [mean values are denoted by orange squares in (a) and (b)]. The parabolic fits for thresholds TO_{-50} (black), and TO_{-100} (red) have *maxima* at 1980.6 and 1982.3, while for TO_{-144} (green) the parabolic fit gives a minimum at 2015.9.

but it seems that the trend reversal for the difference TO series (difference between the ozone concentration inside the polar vortex and its perimeter) is detectable around the point in time when the EESC load started to level-off and later to decrease at the mid-latitudes and polar regions.

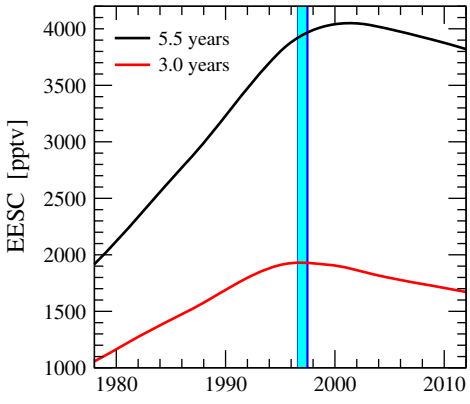

Figure 17. Effective equivalent stratospheric chlorine (EESC) time series for the study period [*Newman et al.*, 2007]. The assumed mean age of air (in the stratosphere) required for the calculation of EESC [*Newman et al.*, 2007] is 5.5 and 3 years, characteristic of the Antarctic region (black) and mid-latitudes (red), respectively. Blue bands indicate the estimated trend reversal for ΔTO_1 and ΔTO_2 by the χ^2 quadratic fitting procedure (cf. Figure 8).

A more accurate attribution of the year of the turnaround in ozone to the turnaround in EESC is not meaningful because of the statistical uncertainties in the turning point of the total ozone time series (see above) and because a one-to-one correspondence between EESC and Antarctic ozone loss is not expected [Kuttippurath et al., 2015; Strahan et al., 2014]. Besides EESC, several confounding factors, such as QBO, volcanic eruptions, long-term dynamical variability, inter-annual variability in polar diabatic descent, and stratospheric temperature fluctuations, certainly contribute to the observed TO changes. Thus, a combination of the results of numerical models with a statistical analysis of observed total ozone in Antarctica might be the way forward to more detailed insights of a trend reversal in Antarctic ozone.

Acknowledgments
We thank Bodeker Scientific for providing the total column ozone database (http://www.bodekerscientific.com/data) and Paul Newman for providing the EESC data (http://acd-ext.gsfc.nasa.gov/). We also thank J. Carter-Sigglow for a grammatical and stylistic revision of the manuscript. This work is supported by the Hungarian Science Foundation under grant number OTKA NK100296, and by the European Commission under grant numbers StratoClim-603557-FP7-ENV.2013.6.1-2 and TAMOP-4.2.2.C-11/1/KONV-2012-0013.

References

Allen, D. R., R. M. Bevilacqua, G. E. Nedoluha, C. E. Randall, and G. L. Manney (2003), Unusual stratospheric transport and mixing during the 2002 Antarctic winter, *Geophys. Res. Lett.*, *30*, L1599, doi:10.1029/2003GL017117.

Bodeker, G. E., B. J. Connor, J. B. Liley, and W. A. Matthews (2001a), The global mass of ozone: 1978–1998, *Geophys. Res. Lett.*, *28*, 2819–2822, doi:10.1029/2000GL012472.

Bodeker, G. E., J. C. Scott, K. Kreher, and R. L. McKenzie (2001b), Global ozone trends in potential vorticity coordinates using TOMS and GOME intercompared against the Dobson network: 1978–1998, *J. Geophys. Res.*, *106*, 23,029–23,042, doi:10.1029/2001JD900220.

Bodeker, G. E., H. Shiona, and H. Eskes (2005), Indicators of Antarctic ozone depletion, *Atmos. Chem. Phys.*, *5*, 2603–2615.

Brainina, I. S. (2013), *Applications of Random Process Excursion Analysis*, Elsevier, London.

Daniel, J. S., S. Solomon, and D. L. Albritton (1995), On the evaluation of halocarbon radiative forcing and global warming potentials, *J. Geophys. Res.*, *100*, 1271–1285, doi:10.1029/94JD02516.

de Laat, A. T. J., R. J. van der A, and M. van Weele (2015), Tracing the second stage of ozone recovery in the Antarctic ozone-hole with a "big data" approach to multivariate regressions, *Atmos. Chem. Phys.*, *15*, 79–97, doi:10.5194/acp-15-79-2015.

Eyring, V., et al. (2010), Multi-model assessment of stratospheric ozone return dates and ozone recovery in CCMVal-2 models, *Atmos. Chem. Phys.*, *10*, 9451–9472.

Farman, J. C., B. G. Gardiner, and J. D. Shanklin (1985), Large losses of total ozone in Antarctica reveal seasonal ClO_x/NO_x interaction, *Nature*, *315*, 207–210.

Grooß, J.-U., P. Konopka, and R. Müller (2005), Ozone chemistry during the 2002 Antarctic vortex split, *J. Atmos. Sci.*, *62*, 860–870.

Hall, T. M., D. W. Waugh, K. A. Boering, and R. A. Plumb (1999), Evaluation of transport in stratospheric models, *J. Geophys. Res.*, *104*(D15), 18,815–18,839, doi:10.1029/1999JD900226.

Hassler, B., G. E. Bodeker, S. Solomon, and P. J. Young (2011), Changes in the polar vortex: Effects on Antarctic total ozone observations at various stations, *Geophys. Res. Lett.*, *38*, L01805, doi:10.1029/2010GL045542.

Ko, M., P. A. Newman, S. Reimann, and S. Strahan (Eds.) (2013), Lifetimes of stratospheric ozone-depleting substances, their replacements, and related species, *SPARC Rep. No. 6, WCRP-15/2013*, SPARC Office, Zurich, Switzerland.

Kuttippurath, J., F. Lefèvre, J.-P. Pommereau, H. K. Roscoe, F. Goutail, A. Pazmiño, and J. D. Shanklin (2013), Antarctic ozone loss in 1979–2010: First sign of ozone recovery, *Atmos. Chem. Phys.*, *13*, 1625–1635.

Kuttippurath, J., G. E. Bodeker, H. K. Roscoe, and P. J. Nair (2015), A cautionary note on the use of EESC-based regression analysis for ozone trend studies, *Geophys. Res. Lett.*, *42*, 162–168, doi:10.1002/2014GL062142.

Lagarias, J. C., J. A. Reeds, M. H. Wright, and P. E. Wright (1998), Convergence properties of the Nelder-Mead simplex method in low dimensions, *SIAM J. Optim.*, *9*, 112–147.

Levelt, P., G. H. J. Van den Oord, M. Dobber, A. Malkki, H. Visser, J. de Vries, P. Stammes, J. Lundell, and H. Saari (2006), The ozone monitoring instrument, *IEEE Trans. Geosci. Remote Sens.*, *44*(5), 1093–1101, doi:10.1109/TGRS.2006.872333.

Mann, M. E., and J. M. Lees (1996), Robust estimation of background noise and signal detection in climatic time series, *Clim. Change*, *33*, 409–445.

Mathews, J. H., and K. K. Fink (2004), *Numerical Methods Using Matlab*, 4th ed., pp. , Prentice Hall, Upper Saddle River, N. J.

McKinnon, K. I. M. (1998), Convergence of the Nelder-Mead simplex method to a non-stationary point, *SIAM J. Optim.*, *9*, 148–158.

Montzka, S. A. (2012), Source gases that affect stratospheric ozone, in *Stratospheric Ozone Depletion and Climate Change*, edited by R. Müller, pp. 33–77, RSC Publishing, London.

Müller, R., J.-U. Grooß, C. Lemmen, D. Heinze, M. Dameris, and G. E. Bodeker (2008), Simple measures of ozone depletion in the polar stratosphere, *Atmos. Chem. Phys.*, *8*, 251–264.

Newman, P. A., E. R. Nash, S. R. Kawa, S. A. Montzka, and S. M. Schauffler (2006), When will the Antarctic ozone hole recover?, *Geophys. Res. Lett.*, *33*, L12814, doi:10.1029/2005GL025232.

Newman, P. A., J. S. Daniel, D. W. Waugh, and E. R. Nash (2007), A new formulation of equivalent effective stratospheric chlorine (EESC), *Atmos. Chem. Phys.*, *7*, 4537–4552.

Press, W. H., S. A. Teukolsky, W. T. Vetterling, and B. P. Flannery (1992), *Numerical Recipes in C*, 2nd ed., pp., Cambridge Univ. Press, Cambridge, U. K.

Rodriguez, J. M., M. K. W. Ko, N. D. Sze, C. W. Heisey, G. K. Yue, and M. P. McCormick (1994), Ozone response to enhanced heterogeneous processing after the eruption of Mt. Pinatubo, *Geophys. Res. Lett.*, *21*(3), 209–212, doi:10.1029/93GL03537.

Salby, M. L., E. A. Titova, and L. Deschamps (2011), Rebound of Antarctic ozone, *Geophys. Res. Lett.*, *38*, L09702, doi:10.1029/2011GL047266.

Salby, M. L., E. A. Titova, and L. Deschamps (2012), Changes of the Antarctic ozone hole: Controlling mechanisms, seasonal predictability, and evolution, *J. Geophys. Res.*, *117*, D10111, doi:10.1029/2011JD016285.

Solomon, S. (1999), Stratospheric ozone depletion: A review of concepts and history, *Rev. Geophys.*, *37*, 417–436, doi:10.1029/1999RG900008.

Stolarski, R. S., A. J. Krueger, M. R. Schoeberl, R. D. McPeters, P. A. Newman, and J. C. Alpert (1986), Nimbus 7 satellite measurements of the springtime Antarctic ozone decrease, *Nature*, *322*, 808–811.

Strahan, S. E., A. R. Douglass, P. A. Newman, and S. D. Steenrod (2014), Inorganic chlorine variability in the Antarctic vortex and implications for ozone recovery, *J. Geophys. Res.*, *119*, 14,098–14,109, doi:10.1002/2014JD022295.

Struthers, H., et al. (2009), The simulation of the Antarctic ozone hole by chemistry-climate models, *Atmos. Chem. Phys.*, *9*, 6363–6376.

Tie, X., and G. Brasseur (1995), The response of stratospheric ozone to volcanic eruptions: Sensitivity to atmospheric chlorine loading, *Geophys. Res. Lett.*, *22*, 3035–3038, doi:10.1029/95GL03057.

Tilmes, S., R. Müller, R. J. Salawitch, U. Schmidt, C. R. Webster, H. Oelhaf, J. M. Russell III, and C. C. Camy-Peyret (2008), Chemical ozone loss in the Arctic winter 1991–1992, *Atmos. Chem. Phys.*, *8*, 1897–1910.

Toms, J. D., and M. L. Lesperance (2003), Piecewise regression: A tool for identifying ecological thresholds, *Ecology*, *84*, 2034–2041.

World Meteorological Organization (WMO) (2011), Scientific assessment of ozone depletion: 2010, *Global Ozone Research and Monitoring Project, Rep. No. 52*, Geneva, Switzerland.

World Meteorological Organization (WMO) (2014), Assessment for decision-makers: Scientific assessment of ozone depletion: 2014, *Global Ozone Research and Monitoring Project, Rep. No. 56*, Geneva, Switzerland.

Yang, E.-S., D. M. Cunnold, M. J. Newchurch, R. J. Salawitch, M. P. McCormick, J. M. Russell, J. M. Zawodny, and S. J. Oltmans (2008), First stage of Antarctic ozone recovery, *J. Geophys. Res.*, *113*, D20308, doi:10.1029/2007JD009675.